Alignment-to-orientation conversion in a magnetic field at nonlinear excitation of the D_2 line of rubidium: Experiment and theory

M. Auzinsh,* A. Berzins, R. Ferber, F. Gahbauer, L. Kalvans, A. Mozers, and A. Spiss
Laser Centre, University of Latvia, Rainis Boulevard 19, LV-1586 Riga, Latvia
(Received 13 March 2015; published 21 May 2015)

We studied alignment-to-orientation conversion caused by excited-state level crossings in a nonzero magnetic field of both atomic rubidium isotopes. Experimental measurements were performed on the transitions of the D_2 line of rubidium. These measured signals were described by a theoretical model that takes into account all neighboring hyperfine transitions, the mixing of magnetic sublevels in an external magnetic field, the coherence properties of the exciting laser radiation, and the Doppler effect. In the experiments, laser-induced fluorescence components were observed at linearly polarized excitation and their difference was taken afterwards. By observing the two oppositely circularly polarized components, we were able to see structures not visible in the difference graphs, which give deeper insight into the processes responsible for these signals. We studied how these signals are dependent on intensity and how they are affected when the exciting laser is tuned to different hyperfine transitions. The comparison between experiment and theory was carried out fulfilling the nonlinear absorption conditions. The theoretical curves described the experimental measurements satisfactorily, reproducing even small features in the shapes of the curves.

DOI: 10.1103/PhysRevA.91.053418 PACS number(s): 32.80.Xx, 32.60.+i

I. INTRODUCTION

The frequency, direction, and polarization of light emitted from an ensemble of atoms are a sensitive probe of their quantum state [1]. Changes in polarization, such as rotation of the plane of polarization, are used to develop sensitive magnetometers [2]. Other uses of nonlinear magneto-optical resonances include electromagnetically induced transparency [3], information storage using light [4,5], atomic clocks [6], optical switches [7], filters [8], and isolators [9].

When linearly polarized light interacts with an ensemble of atoms, it usually aligns the angular momentum of the atoms in the excited state as well as in the ground state. Angular momentum alignment can be symbolically represented by a double-headed arrow. If the angular momentum of the atoms is aligned along the quantization axis (longitudinal alignment), the populations of magnetic sublevels with quantum number $+m_F$ and $-m_F$ are equal, but the population may vary as a function of $|m_F|$. But if the angular momentum is aligned perpendicularly to the quantization axis (transverse alignment), then, in quantum terms, it means that there is coherence between magnetic sublevels with quantum numbers that differ by $\Delta m_F = 2$ (see Fig. 1).

In a similar way, we can introduce the longitudinal and transverse orientation of angular momentum. In the case of orientation of the angular momentum, the spatial distribution can be represented symbolically by a single-headed arrow, and in the case of longitudinal orientation, the magnetic sublevels with quantum numbers $+m_F$ and $-m_F$ in general have different populations. However, the case of transverse orientation corresponds to coherence between magnetic sublevels with values that differ by $\Delta m_F = 1$ (see Fig. 1).

Since an aligned ensemble of atoms defines a preferred axis but no preferred direction in space, the fluorescence emitted by an aligned state can be polarized only linearly [10]. An oriented ensemble of atoms, on the other hand, does define a preferred orientation in space, and thus can emit circularly polarized radiation.

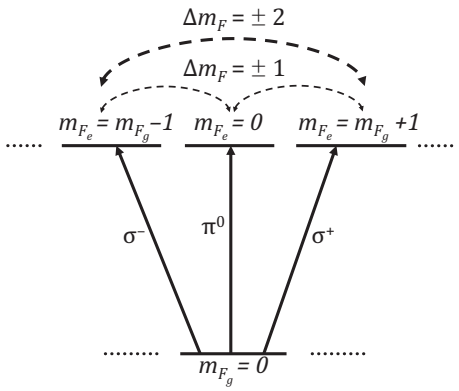

FIG. 1. Absorption from the ground-state hyperfine magnetic sublevel m_{F_g} and creation of $\Delta m_F = 1$ and $\Delta m_F = 2$ coherences in the excited state when the magnetic field $B = 0$.

Alignment created by linear polarized excitation can be converted to orientation by external interactions such as a magnetic field gradient [11] or anisotropic collisions [12–14]. This process is called alignment-to-orientation conversion (AOC) [15]. Interaction with an electric field also can produce orientation from an initially aligned population [16]. A magnetic field by itself cannot create orientation from alignment because it is an axial field that is symmetric under reflection in the plane perpendicular to the field direction. However, the hyperfine interaction can cause a nonlinear dependence of the energies of the magnetic sublevels on the magnitude of the magnetic field—the nonlinear Zeeman effect (see Figs. 2 and 3), and this nonlinear dependence can break the symmetry. If, in addition, the linearly polarized exciting radiation can be decomposed into linearly (π^0) and circularly ($\sigma^{\pm}$) polarized components with respect to the quantization axis (see Fig. 4), then $\Delta m_F = 1$ coherences can

*marcis.auzins@lu.lv

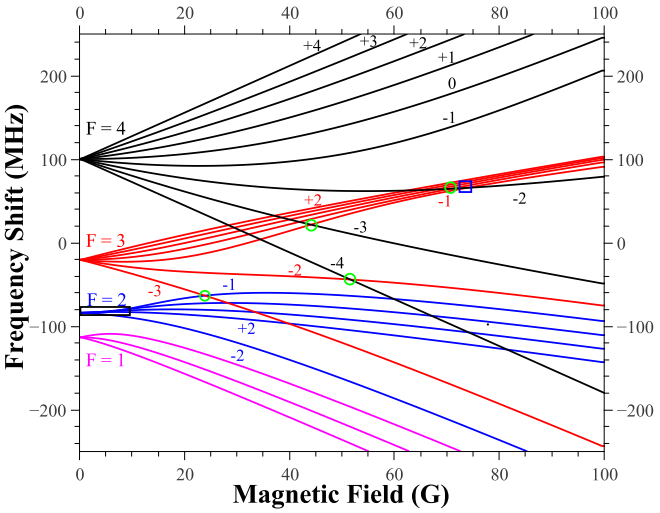

FIG. 2. (Color online) Frequency shifts of the magnetic sublevels m_F of the excited-state fine-structure level $5^2P_{3/2}$ as a function of magnetic field for ^{85}Rb. Zero-frequency shift corresponds to the excited-state fine-structure level $5^2P_{3/2}$. The numbers above the lines correspond to the values of m_F. Level crossings are marked by squares for $\Delta m_F = 1$ and circles for $\Delta m_F = 2$.

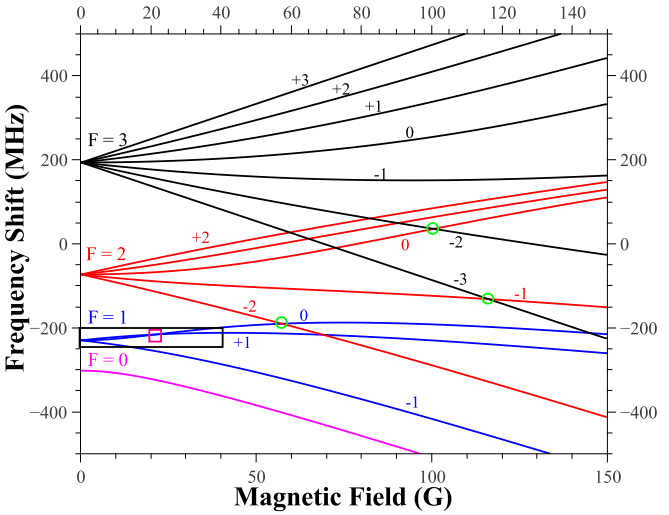

FIG. 3. (Color online) Frequency shifts of the magnetic sublevels m_F of the excited-state fine-structure level $5^2P_{3/2}$ as a function of magnetic field for ^{87}Rb. Zero-frequency shift corresponds to the excited-state fine-structure level $5^2P_{3/2}$. The numbers above the lines correspond to the values of m_F. Level crossings are marked by squares for $\Delta m_F = 1$ and circles for $\Delta m_F = 2$.

be created, which leads to orientation in a direction transverse to the initial alignment. AOC in an external magnetic field was first studied theoretically for cadmium [17] and sodium [18], and observed experimentally in cadmium [19] and in the D_2 line of rubidium atoms [20]. Also the conversion in the opposite sense—conversion of an oriented state into an aligned state—is possible [21]. Nevertheless, the action of external perturbations can break the symmetry of the population distribution and allow linearly polarized exciting radiation to produce orientation, which is manifested by the presence of circularly polarized fluorescence.

Earlier, AOC in rubidium atoms was studied at excitation with weak laser radiation in the linear absorption regime [10]. The perturbing factor in that case was the joint action of the hyperfine interaction and the external magnetic field, which led to nonlinear splitting of the Zeeman magnetic sublevels. The magnetic sublevels of the excited-state angular momentum hyperfine levels in Rb atoms in an external magnetic field already start to be affected by the nonlinear Zeeman effect at moderate field strengths of several tens of Gauss. It should be noted that the ground-state Zeeman effect is linear and so the ground-state magnetic sublevels do not cross.

However, many practical and experimental applications require higher-intensity excitation, in which case the absorption becomes nonlinear. As a result, the theoretical description is no longer simple and requires sophisticated methods in order to predict changes in the degree of circular polarization, which reaches maximum values on the order of only a few percent. Therefore, we have applied a theoretical model developed for the description of such magneto-optical effects, such as dark and bright resonances, to describe the experimental signals of AOC in the D_2 line of rubidium. Because the splittings between the excited-state hyperfine levels are of the order of tens of megahertz for both rubidium isotopes (see Fig. 5), the D_2 line is a very good candidate for demonstrating AOC phenomena at relatively low magnetic fields. The model satisfactorily calculates the degree of polarization for magnetic fields up to at least 85 Gauss, making it a powerful tool for experiments that deal with these effects.

We studied the AOC phenomenon experimentally by exciting the D_2 line of rubidium with linearly polarized light for the case of nonlinear absorption and modeled the line shapes of the resulting magneto-optical signals theoretically. Both circularly polarized components of the fluorescence were recorded in the experiment, rather than just the difference as was done earlier [10]. Moreover, in the present study, the magnetic field range was markedly extended in comparison to previous studies [10], which allowed us to reveal additional signal structure.

II. EXPERIMENT

Rubidium atoms in a vapor cell at room temperature were excited with linearly polarized light whose polarization

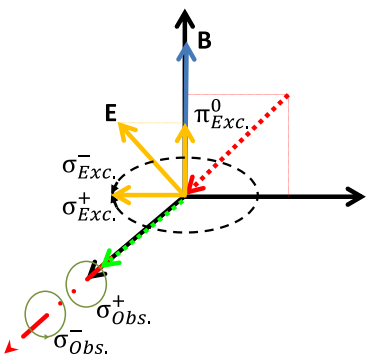

FIG. 4. (Color online) Excitation and observation geometry.

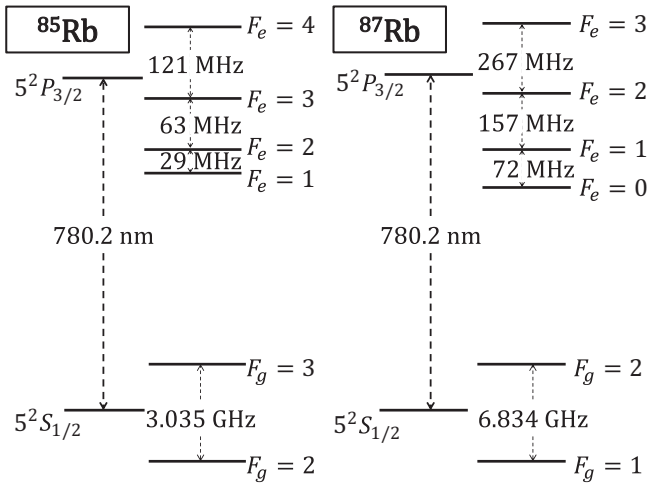

FIG. 5. Fine and hyperfine energy-level splittings for the D_2 transitions of ^{85}Rb and ^{87}Rb.

vector made a 45° angle with an externally applied magnetic field. Laser-induced fluorescence (LIF) was observed in the direction perpendicular to the plane containing the magnetic field **B** and the electric field vector **E** of the exciting radiation (see Fig. 4) [22]. The fluorescence in the observation direction passed through a two-lens system. Between the two lenses, a zero-order quarter-wave plate (Thorlabs WPQ10M-780) converted circularly polarized light into linearly polarized light. Next, a linear polarizer served as an analyzer, which allowed one or another circularly polarized fluorescence component to pass, depending on the relative angle between the analyzer axis and the fast axis of the quarter-wave plate.

The experimental apparatus is shown schematically in Fig. 6. Rubidium atoms from a natural isotopic mixture were contained in a cylindrical Pyrex cell (length and diameter both 25 mm) with optical quality windows. The rubidium cell was located at the center of three pairs of mutually orthogonal Helmholtz coils. The magnetic field was scanned in the z direction, while the two remaining coils were used to compensate the ambient static magnetic field. We estimate

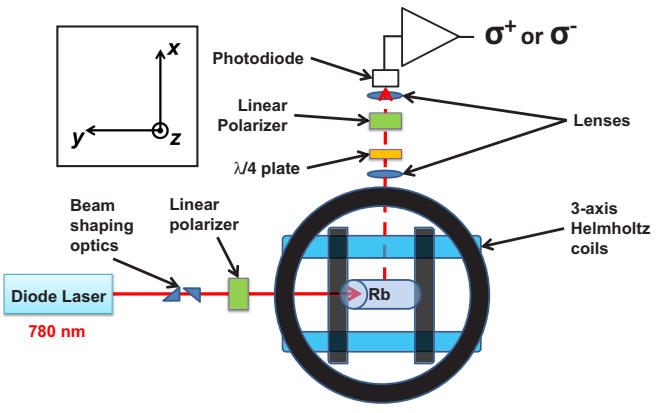

FIG. 6. (Color online) Top view of the experimental setup. Although in the top view it appears that the beam is parallel to the y axis, in fact it enters the coils at an angle of 45° with respect to the y axis in the yz plane.

that the ambient magnetic field was compensated to better than 0 ± 20 mG. In order to scan the magnetic field in both directions, a bipolar power supply (Kepco BOP-50-8-M) was used, reaching magnetic field values of 85 G in both directions.

The laser used in these experiments was a Toptica DL Pro grating-stabilized, tuneable, single-mode diode laser. The frequency of the laser excitation was stabilized by generating a saturated absorption spectrum and locking the laser frequency to a saturated absorption peak in this signal using a Toptica DigiLock 110 feedback control module. The frequency was additionally monitored by a HighFinesse WS/7 Wavemeter. The temperature and current of the laser were controlled by Toptica DTC 110 and DCC 110 controllers, respectively.

The diameter of the beam was 1.90 mm at the full width at half maximum (FWHM) as determined from the Gaussian fit obtained by a beam profiler (Thorlabs BP104-VIS). The ellipticity of the laser beam was compensated by an anamorphic prism pair. The laser power was changed using neutral density filters placed before the linear polarizer. The LIF of the two opposite circularly polarized light components was collected on a photodiode (Thorlabs FDS100). Each component was measured separately and multiple scans were acquired and averaged before switching the analyzing polarizer in order to measure the orthogonally polarized component. The signal was amplified by a transimpedance amplifier based on a TL072 op-amp with a gain of 10^6 followed by a voltage amplifier with a gain of 10^4 (Roithner multiboard). The signals were stored after each scan on a PC using an Agilent DSO5014A oscilloscope. A residual misalignment in the experimental setup introduced a slight asymmetry in the signal, but it could be eliminated by averaging the signals recorded for positive and negative values of magnetic field.

In order to compare experiment with theory, both components were normalized to the maximum of the σ^+ component, making it possible to compare the relative intensities of the two components in arbitrary units. The background was measured in two different ways: by detuning the laser frequency from resonance and by blocking the laser beam. Both produced equal results. In the fitting process, a constant background was introduced, which was close to the experimentally measured background. The experimental results were very sensitive to any slight misalignment of the analyzing polarizer that could distort the measured strengths of each circular polarization component. Therefore, to find the best agreement between experiment and theory, a parameter was varied that represented the relative strength of each experimentally measured fluorescence component. This factor was usually around 10% and never more than 22%.

III. THEORETICAL MODEL

A well-tested model based on optical Bloch equations (OBEs) that are solved for steady-state excitation conditions is used to describe the experiment theoretically. The ensemble of rubidium atoms is described by a quantum density matrix ρ that is written in the basis ξ, F_i, m_{F_i}, where F_i denotes the quantum number of the total atomic angular momentum including nuclear spin I for either the ground ($i = g$) or the excited ($i = e$) state, m_{F_i} is the magnetic quantum number, and ξ stands for all the other quantum numbers that are irrelevant

in the context of our experiment. Thus, the general OBEs [23],

$$i\hbar\frac{\partial\rho}{\partial t} = [\hat{H},\rho] + i\hbar\hat{R}\rho, \tag{1}$$

can be transformed into explicit rate equations for the Zeeman coherences within the ground ($\rho_{g_i g_j}$) and excited ($\rho_{e_i e_j}$) states, respectively. To do so, the laser radiation is described as a classically oscillating electric field $\mathbf{E}(t)$ with a stochastically fluctuating phase. Thus, the interaction operator can be written in the dipole approximation with dipole operator $\hat{\mathbf{d}}$,

$$\hat{V} = -\hat{\mathbf{d}}\cdot\mathbb{E}(t). \tag{2}$$

The interaction with the magnetic field is described by the operator

$$\hat{H}_B = \frac{\mu_B}{\hbar}(g_J\mathbf{J} + g_I\mathbf{I})\cdot\mathbf{B}, \tag{3}$$

where $\mathbf{J}$ and $\mathbf{I}$ are, respectively, the total electronic angular momentum and nuclear spin, which together make up the total atomic angular momentum $\mathbf{F}$. The quantities g_J and g_I are the respective Landé factors, $\mathbf{B}$ is the external magnetic field, μ_B is Bohr's magneton, and $\hbar$ is Planck's constant. The matrix elements for the electric dipole transition can be written in explicit matrix form with the help of the Wigner-Eckart theorem [24].

Thus, the total interaction Hamiltonian in (1) is

$$\hat{H} = \hat{H}_0 + \hat{H}_B + \hat{V}, \tag{4}$$

where H_0 governs the internal energy of an unperturbed atom.

The relaxation operator in (1) includes terms for the spontaneous relaxation rate Γ and the transit relaxation rate γ, which is the inverse of the average time an atom takes to traverse the laser beam.

By applying the rotating-wave approximation, averaging over and decorrelating from the stochastic phases, and eliminating the optical coherences as described in detail by Blush and Auzinsh [25], the rate equations for the Zeeman coherences are obtained:

$$\frac{\partial\rho_{g_i g_j}}{\partial t} = \left(\Xi_{g_i e_m} + \Xi^*_{g_j e_k}\right)\sum_{e_k,e_m} d^*_{g_i e_k} d_{e_m g_j}\rho_{e_k e_m} - \sum_{e_k,g_m}\left(\Xi^*_{g_j e_k} d^*_{g_i e_k} d_{e_k g_m}\rho_{g_m g_j} + \Xi_{g_i e_k} d^*_{g_m e_k} d_{e_k g_j}\rho_{g_i g_m}\right)$$
$$- i\omega_{g_i g_j}\rho_{g_i g_j} - \gamma\rho_{g_i g_j} + \sum_{e_k e_l}\Gamma^{e_k e_l}_{g_i g_j}\rho_{e_k e_l} + \lambda\delta(g_i,g_j), \tag{5a}$$

$$\frac{\partial\rho_{e_i e_j}}{\partial t} = \left(\Xi^*_{g_m e_i} + \Xi_{g_k e_j}\right)\sum_{g_k,g_m} d_{e_i g_k} d^*_{g_m e_j}\rho_{g_k g_m} - \sum_{g_k,e_m}\left(\Xi_{g_k e_j} d_{e_i g_k} d^*_{g_k e_m}\rho_{e_m e_j} + \Xi^*_{g_k e_i} d_{e_m g_k} d^*_{g_k e_j}\rho_{e_i e_m}\right) - i\omega_{e_i e_j}\rho_{e_i e_j} - (\Gamma+\gamma)\rho_{e_i e_j}. \tag{5b}$$

The first two terms in both equations describe the population increase or decrease and the creation of Zeeman coherences within the respective atomic states due to the interaction of atoms with the laser radiation. The elements of the transition dipole matrix are given by d_{ij} [obtained from (2)], and Ξ_{ij}, which is defined below in Eq. (6), gives the atom-field interaction strength. The third term of the rate equations (5) describes the destruction of coherence by the magnetic field, and ω_{ij} is the energy difference between magnetic sublevels $|i\rangle$ and $|j\rangle$ and can be obtained by diagonalizing the matrix $\hat{H}_0 + \hat{H}_B$. The fourth term describes the population loss and destruction of coherence caused by relaxation. The fifth term in (5a) describes repopulation of the ground state by spontaneous transitions and the sixth term describes repopulation by transit relaxation. If we assume that the atomic density matrix outside the interaction region is normalized, then $\lambda = \frac{1}{n_g}\gamma$, where n_g is the total number of magnetic sublevels in the ground state.

The quantity $\Xi_{g_i e_j}$ in Eq. (5) describes the strength of interaction between the laser radiation and the atoms and is expressed as follows:

$$\Xi_{g_i e_j} = \frac{\Omega_R^2}{\frac{\Gamma+\gamma+\Delta\omega}{2} + i\left(\bar{\omega} - \mathbf{k}_{\bar{\omega}}\cdot\mathbf{v} + \omega_{g_i e_j}\right)}, \tag{6}$$

where Ω_R is the reduced Rabi frequency, used as a theoretical parameter that corresponds to the intensity in the experiment, $\Delta\omega$ is the finite spectral width of the exciting radiation, $\bar{\omega}$ is the central frequency of the exciting radiation, $\mathbf{k}_{\bar{\omega}}$ is the wave vector of exciting radiation, and $\mathbf{k}_{\bar{\omega}}\mathbf{v}$ is the Doppler shift experienced by an atom moving with velocity $\mathbf{v}$.

If we are interested in steady-state conditions such as obtained during the experiment, it is possible to obtain the optical coherences from the optical Bloch equations in terms of the Zeeman coherences [25]. The validity of this approach is further bolstered by the fact that an atom with the most probable thermal velocity takes about 8 microseconds to traverse the laser beam of nominal diameter 1.9 mm (FWHM). Since we consider Rabi frequencies on the order of 1 MHz, the rate of transiting the beam is still significantly lower than the Rabi frequency, even for atoms that traverse only half the nominal beam diameter, and the fraction of atoms whose path length in a circular beam is less than half the nominal diameter is 13.4% [26]. Thus, we can apply steady-state conditions

$$0 = \frac{\partial\rho_{g_i g_j}}{\partial t} = \frac{\partial\rho_{e_i e_j}}{\partial t}, \tag{7}$$

obtaining from (5) a set of linear equations that can be solved numerically to obtain the density-matrix components that correspond to the population and the Zeeman coherences of the ground and excited states. Once the density matrix is known, we use the following expression to obtain the intensity (up to a constant factor I_0) of an arbitrary polarized fluorescence

component with polarization denoted by **e** [15,27,28]:

$$I_{fl}(\mathbf{e}) = \tilde{I}_0 \sum_{g_i,e_j,e_k} d^{*(ob)}_{g_i e_j} d^{(ob)}_{e_k g_i} \rho_{e_j e_k}. \tag{8}$$

To include the effects of the thermal motion of the atoms, we perform Riemann integration over the velocity distribution by solving Eqs. (5) and evaluating (8) for each atomic velocity group.

To fit the theoretical and experimental results, we estimate and fine tune the following parameters: transit relaxation rate γ, reduced Rabi frequency Ω_R, and spectral width of the laser radiation $\Delta\omega$.

The estimation of the transit relaxation rate is straightforward,

$$\gamma = \frac{v_{th}}{d}, \tag{9}$$

where v_{th} is the mean thermal velocity of the atoms projected onto the plane perpendicular to the laser beam and d is the laser-beam diameter, which in the theoretical model is assumed to be cylindrical in shape with uniform intensity. For $d = 1900\ \mu$m and $T = 293$ K, we obtain $\gamma = 2\pi(0.018$ MHz).

The Rabi frequency can be estimated theoretically as

$$\Omega_R = k_R \frac{||d|| \cdot |\varepsilon|}{\hbar} = k_R \frac{||d||}{\hbar} \sqrt{\frac{2I}{\epsilon_0 n c}}, \tag{10}$$

where $||d|| = 5.977 e a_0$ [1] is the the D_2 transition reduced dipole matrix element, with e as the electron charge and a_0 as the Bohr radius [24], I is the intensity (directly related to the amplitude of the electric field $|\varepsilon|$), ϵ_0 is the electric constant, n is the refractive index, c is the speed of light, and k_R is a fitting constant. In the ideal case of a homogeneous beam, k_R would be unity. In practice, the intensity I is not constant across the laser beam and it is defined somewhat arbitrarily as the power in the laser beam divided by the cross-sectional area of the beam at the FWHM. The theoretical model, however, admits only one value for the Rabi frequency, in practice assuming a constant intensity over the beam. As a result, the value of the Rabi frequency used in the model is adjusted by the fitting constant k_R. Furthermore, in the idealized beam, the relationship between Ω_R^2 and I would be linear. However, previous experience [29,30] suggests that this linear relationship should not hold for all values of the intensity in a real experiment with a Gaussian beam. In fact, in our experiment, the value of k_R ranged from 0.27 for lower intensities to 0.15 for higher intensities.

The complicated relationship between I and Ω_R has a simple explanation. Our experiment was performed in the regime of nonlinear absorption, which implies that for large laser intensities, the ground-state population is strongly depleted. When one starts to gradually increase laser intensity, initially the ground-state population is only slightly changed even at the center of the beam, where the light is most intense. When the intensity is increased still more, the ground-state population at the center of the beam starts to be depleted significantly. When the intensity is increased further, there is little ground-state population left in the beam center, and the region of population depletion expands to the "wings" of the Gaussian intensity distribution, which can extend a significant distance from the laser beam's center.

As a consequence of this spatially dependent population depletion, for weaker laser radiation, the main contribution to the signal comes from the central parts of the laser beam where we have the strongest intensity, even though the theoretical proportionality of Ω_R to the square root of intensity continues to hold. In contrast, for stronger laser radiation, the peripheral parts of the laser beam, where the radiation intensity is smaller, start to play a larger role in the absorption process because only there is the ground-state population still significant. In each of these cases, the radiation intensity in different parts of the beam plays a dominant role in the absorption process and should be related to the value of the Rabi frequency that appears in the rate equations for the density matrix. Thus we vary the value of coefficient k_R in order to account for this effect and to achieve better correspondence between experiment and theory.

A value of $\Delta\omega = 2\pi(1$ MHz) was found to be an appropriate estimate for the spectral width of the laser and is close to the value given by the manufacturer of the laser.

IV. RESULTS AND DISCUSSION

Before the experiments were carried out, some preliminary theoretical calculations were performed in order to deduce which hyperfine transition would yield the most noticeable signals related to the AOC phenomenon in both rubidium isotopes. A good measure of the strength of the AOC effect is the degree of circularity of the laser-induced fluorescence, defined as $(I_{\sigma^+} - I_{\sigma^-})/(I_{\sigma^+} + I_{\sigma^-})$. The theoretical calculations predicted that the largest circularity signal (4%) would be observed for ^{85}Rb when excited from the second ground-state hyperfine level $F_g = 2$ to the second excited-state hyperfine level $F_e = 2$. As seen in Fig. 7, because of Doppler broadening, the signal did not depend significantly on which excited-state hyperfine level was excited when the excitation took place from the ground-state hyperfine level with $F_g = 2$. The observable circularity for the other transitions was predicted to be 1% or less. For the case of ^{87}Rb, the $F_g = 1 \longrightarrow F_e = 1$ transition was selected because the predicted circularity degree was 1%, whereas for excitation from the other ground-state hyperfine level $F_g = 2$, the circularity degree was predicted to be less than 1%. Therefore, we concentrated our experimental efforts on the $F_g = 2 \longrightarrow F_e = 2$ transition of ^{85}Rb and the $F_g = 1 \longrightarrow F_e = 1$ transition of ^{87}Rb.

Figure 8 shows a typical result for the $F_g = 2 \longrightarrow F_e = 2$ transition of ^{85}Rb. Figures 8(a) and 8(b) depict the two orthogonally circularly polarized fluorescence components. When the magnetic field value is zero, all magnetic sublevels m_F that belong to the same F level in the excited and ground states are degenerate, giving a typical dark resonance for the $F_g = 2 \longrightarrow F_e = 2$ transition of ^{85}Rb [31]. As the magnetic field magnitude increases, these sublevels shift according to the nonlinear Zeeman effect (Fig. 2), thereby destroying the aligned state and allowing more laser light to be absorbed, which causes a rapid rise in the fluorescence signal. After that, the overall signal tendency is to diminish as the magnetic field strength increases, apart from two small peaks at about 23 and 44 G.

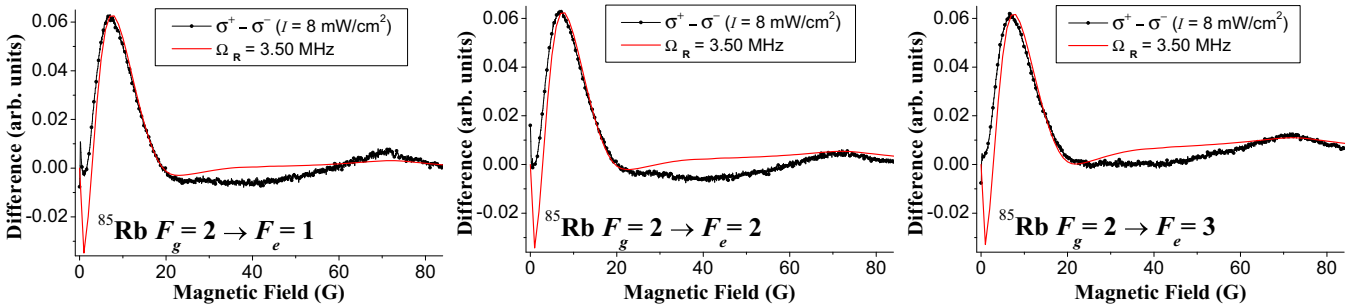

FIG. 7. (Color online) Signal dependence on the excited-state hyperfine level F_e to which the laser is tuned when excited from the ground-state hyperfine level $F_g = 2$ of ^{85}Rb. The left-most plot shows the difference between the two oppositely circularly polarized components ($I_{\sigma^+} - I_{\sigma^-}$) for the $F_g = 2 \longrightarrow F_e = 1$ transition, the center plot shows the difference ($I_{\sigma^+} - I_{\sigma^-}$) for the $F_g = 2 \longrightarrow F_e = 2$ transition, and the third plot (right-most) corresponds to the $F_g = 2 \longrightarrow F_e = 3$ transition. The smooth, red curve is theory and the black filled circles connected by a black line are the experimental data, with only every tenth point shown.

These two small peaks can be attributed to $\Delta m_F = 2$ coherences. The 23 G peak appears because the $m_F = -1$ sublevel of the $F_e = 2$ hyperfine level crosses the $m_F = -3$ sublevel of the $F_e = 3$ hyperfine level (see Fig. 2), thus creating a $\Delta m_F = 2$ coherence. The other small peak at 44 G can be attributed to the crossing of $m_F = -1$ sublevel of the $F_e = 3$ and the $m_F = -3$ sublevel of $F_e = 4$. Note that these peaks are invisible both in the difference signal [Fig. 8(c)] as well as in the circularity signal [Fig. 8(d)] since they cancel each other when the difference is taken.

Besides these two small peaks in the component graphs, there are two peaks at 7 and 74 G in the difference and circularity graphs [Figs. 8(c) and 8(d)] corresponding to the two broader structures in the component graphs [Figs. 8(a) and 8(b)]: one around 6–10 G and another, barely visible one around 70–74 G. These peaks can be attributed to $\Delta m_F = 1$ coherences. The 7 G peak appears as an increase in the signal in one component [Fig. 8(a)] and a decrease in the other [Fig. 8(b)]. Note that their corresponding maximum and minimum values are relatively shifted, giving values of 6 G [Fig. 8(a)] and 9 G [Fig. 8(b)], respectively, in the component graphs. The relative shift of these values can be explained by the fact that this peak is related to three $\Delta m_F = 1$ and two $\Delta m_F = 2$ coherences in the range from 0 to 10 G (see Fig. 9). As we take the difference between the two oppositely circularly polarized components, we can eliminate the $\Delta m_F = 2$ coherences from the signal and thus see the peaks that correspond only to the $\Delta m_F = 1$ crossings. The 74 G peak in Fig. 8(c) can be explained in a similar way. A barely visible structure in the component graphs appears as a broad peak in the difference graph. This peak is related to a single $\Delta m_F = 1$ crossing of the $m_F = -1$ sublevel of $F_e = 3$ and the $m_F = -2$ sublevel of $F_e = 4$, and as a result its

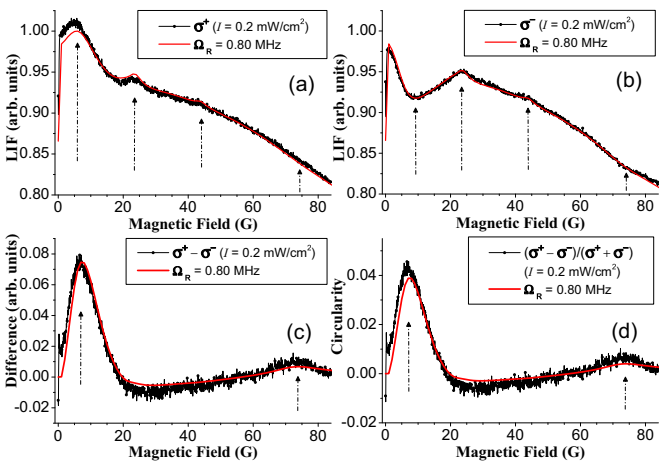

FIG. 8. (Color online) (a),(b) Relative intensities of the two oppositely circularly polarized fluorescence components, (c) their difference, and (d) the circularity value for the $F_g = 2 \longrightarrow F_e = 2$ transition of ^{85}Rb (80 scans averaged). Arrows denote the positions of peaks and maximum (or minimum) values of broader structures. The smooth, red curve is theory and the black filled circles connected by a black line are the experimental data, with only every tenth point shown.

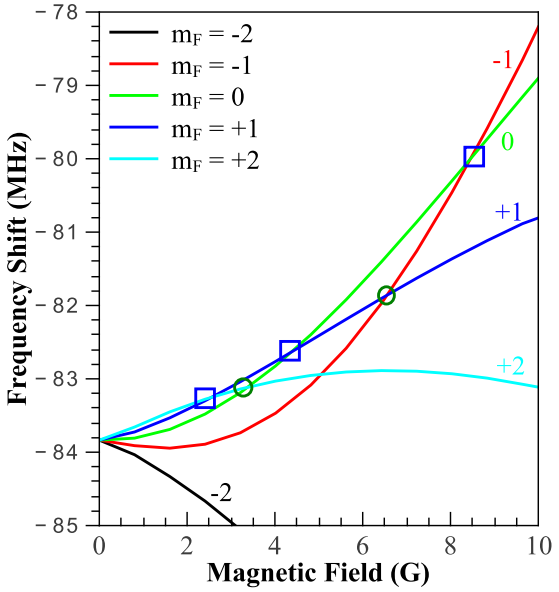

FIG. 9. (Color online) Energy shifts of the magnetic sublevels m_F as a function of magnetic field for ^{85}Rb in the magnetic field range $0 < B < 10$ G. The m_F values are written next to the curves. Squares denote $\Delta m_F = 1$ crossings and circles denote $\Delta m_F = 2$ crossings.

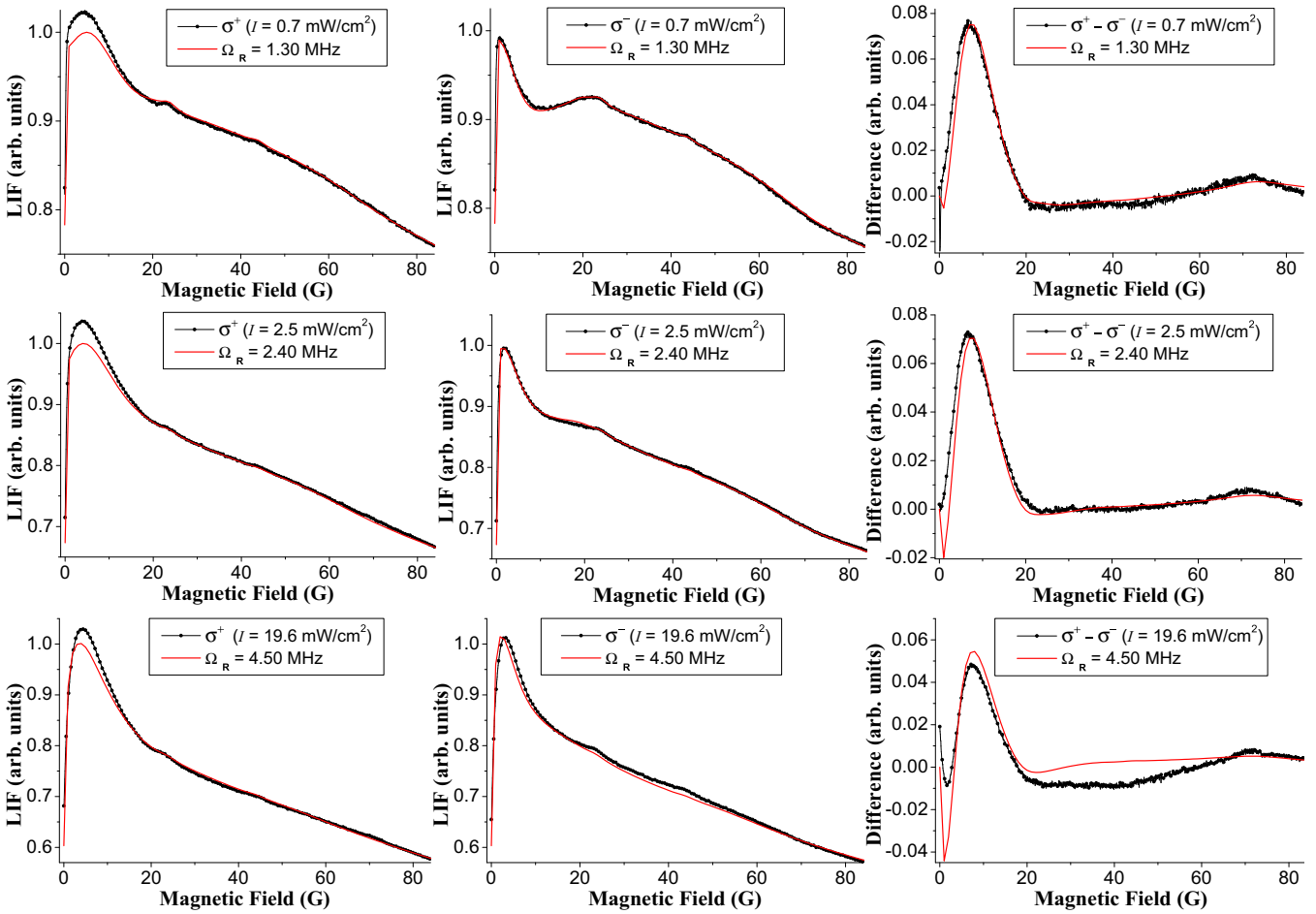

FIG. 10. (Color online) Signal dependence on intensity for excitation of the $F_g = 2 \longrightarrow F_e = 2$ transition of the D_2 line of ^{85}Rb. The plots are organized in columns: relative intensities of the two oppositely circularly polarized fluorescence components are shown in the left and center columns and their difference is shown in the right-most column. The smooth, red curve is theory and the black filled circles connected by a black line are the experimental data, with only every tenth point shown.

amplitude is smaller. The peak is broad because the $m_F = -1$ and $m_F = -2$ sublevels that cross are energetically close to each other ($\Delta E \leqslant 20$ MHz) all the way from 60 to 90 G, as can be seen in Fig. 2.

Figure 10 shows the signal dependence on laser power for the $F_g = 2 \longrightarrow F_e = 2$ transition. One can see in the figure that as the laser power is increased, the broad structures, attributed to $\Delta m_F = 1$ coherences in the component graphs, become less and less pronounced. However, they are still visible in the difference graphs (Fig. 10, right column), although the amplitude slightly decreases, and the sign of the difference signal becomes negative for the $\Omega_R = 4.50$ MHz (19.6 mW/cm^2) case (bottom right in Fig. 10).

Figure 11 shows the signal dependence on laser power for the $F_g = 1 \longrightarrow F_e = 1$ transition of the D_2 line of ^{87}Rb. As the magnetic field is increased, after the initial increase of the signal due to the dark resonance at 0 G, the signal gradually diminishes. However, two small peaks around 45 and 57 G and a broad structure between 7 and 26 G are visible in the component graphs (Fig. 11, left and center columns). The structures visible in the graph of the difference signal (Fig. 11, right column) must be related to $\Delta m_F = 1$ coherences. Indeed, the magnetic sublevels $m_F = 0$ and $m_F = +1$ of $F_e = 1$ cross at 21 G, giving rise to the broad structure from 7 to 26 G (see Fig. 12).

The small peak at 57 G is caused by the crossing of $m_F = 0$ of $F_e = 1$ and $m_F = -2$ of $F_e = 3$ (see Fig. 3), which allows $\Delta m_F = 2$ coherences to be created. As a result, one can observe a small rise in the component LIF signals. This peak should vanish as the difference of the components is taken, since it is related to a $\Delta m_F = 2$ coherence. In the calculated curve, it indeed vanishes, but remains in the measured curve. Possible explanations could be higher-order nonlinear effects not treated by the model or even small experimental imperfections.

The small peak at 45 G in the component graphs cannot be attributed to any crossing in the excited or ground states. The fact that it is visible in the difference graphs might suggest that it is connected to a $\Delta m_F = 1$ coherence. However, theoretical calculations show that when the Zeeman coherences in the density matrix are "turned off," this peak remains, which suggests that it is not connected to any coherences. While the precise origin of the peak remains unknown, the appearance of this peak in both theory and experiment explicitly shows two things: (i) how nonlinear these signals are and (ii) how well the theoretical model works in describing them.

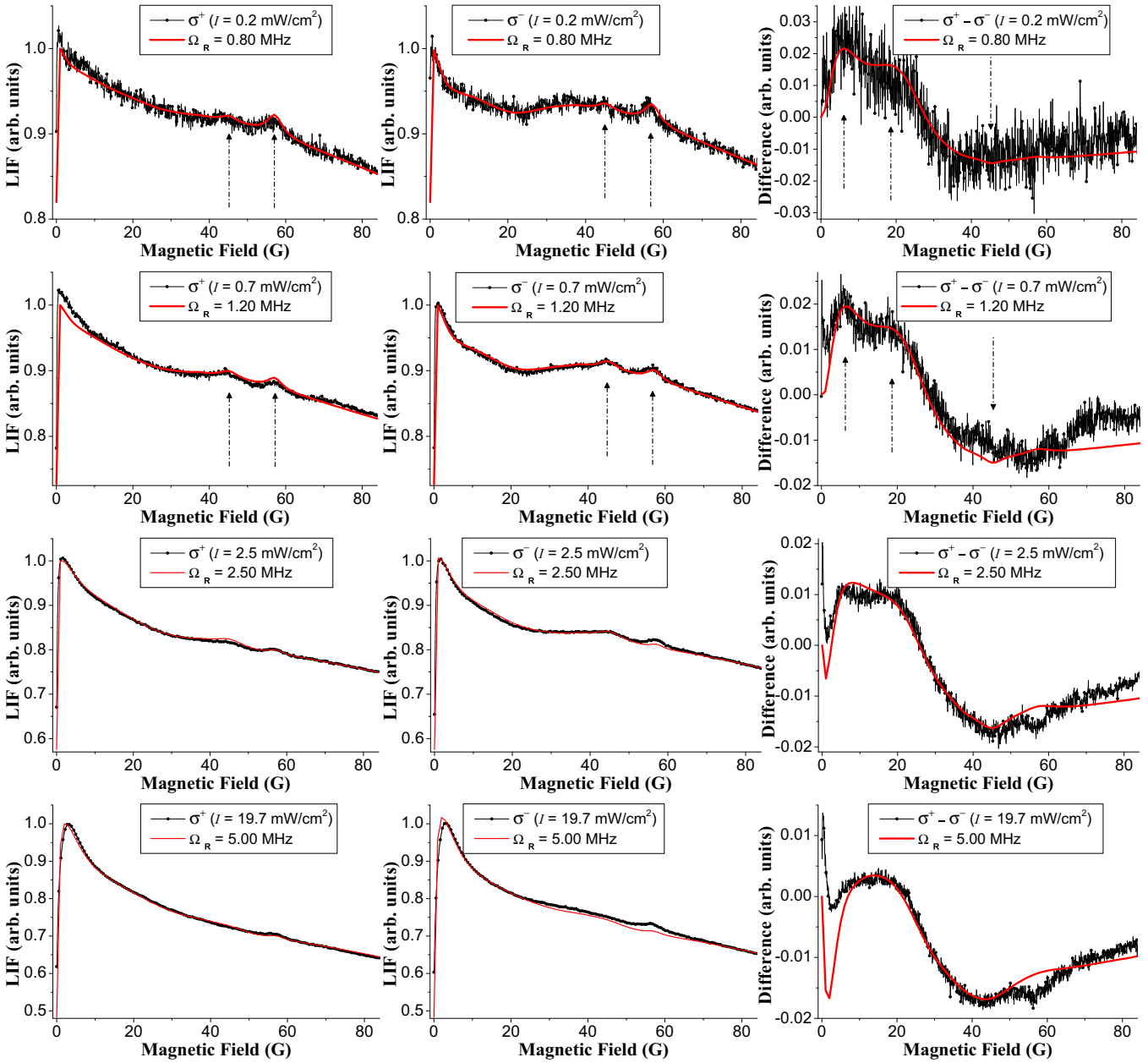

FIG. 11. (Color online) Signal dependence on intensity for excitation of the $F_g = 1 \longrightarrow F_e = 1$ transition of the D_2 line of ^{87}Rb. The plots are organized in columns: relative intensities of the two oppositely circularly polarized fluorescence components are shown in the left and center columns and their difference in the right-most column. Arrows denote the positions of peaks and maximum values of broader structures. The smooth, red curve is theory and the black filled circles connected by a black line are the experimental data, with only every tenth point shown.

For each value of the intensity, the theoretical curve which best described the results of the experiment was selected. Figure 13 shows that the choices made to achieve the best agreement were not arbitrary, but resulted in values that obey the expected relationship between intensity and Rabi frequency. The intensity is plotted against the square of the Rabi frequency for which the best fit of the calculated curve to experimental measurements was obtained. The points should lie on a straight line, and, indeed, they all fall close to the best-fit line with a reduced χ^2 value of 1.4. We note that the relative errors increase at larger intensities because the dependence of the signal on Rabi frequency is not as pronounced for large Rabi frequencies. We may conclude that, at least up to these intensity values, the reduced Rabi frequency Ω_R is proportional to the square root of the intensity I.

V. CONCLUSION

We have carried out experiments with laser-power densities that fulfill the nonlinear absorption conditions and developed a theoretical model that describes AOC under these conditions. The increased magnetic fields and the detection of individual circularly polarized light components in the experiments let us see the structure of the signal in more detail than before [10].

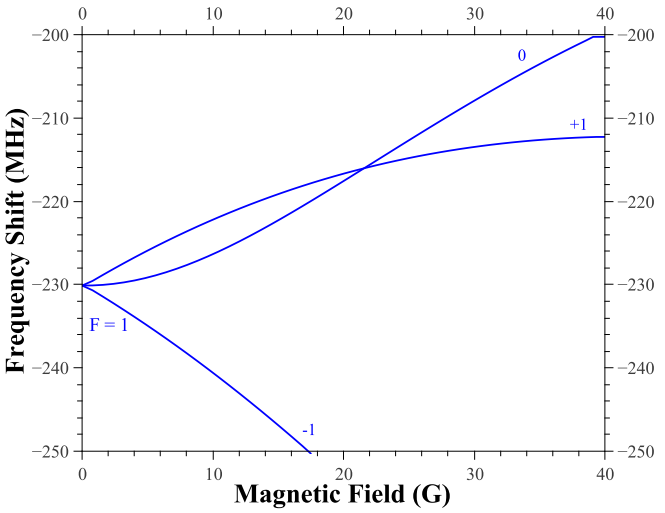

FIG. 12. (Color online) Energy shifts of the magnetic sublevels m_F as a function of magnetic field for ^{87}Rb in the magnetic field range $0 < B < 40$ G. The m_F values are written next to the curves. The square denotes a $\Delta m_F = 1$ crossing.

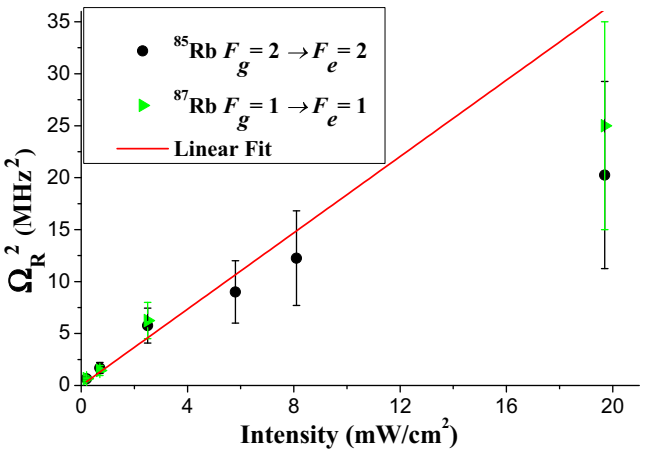

FIG. 13. (Color online) Dependence of the squared Rabi frequency Ω_R^2 on the intensity I together with a linear fit for the transition $F_g = 2 \longrightarrow F_e = 2$ in ^{85}Rb and the transition $F_g = 1 \longrightarrow F_e = 1$ in ^{87}Rb.

With one small exception in Fig. 11, all details, even very small ones, predicted by the theory were reproduced by the experiment and were shown to be related to features of the level-crossing diagrams. Their positions and relative amplitudes match satisfactorily. The signal dependence on intensity shows that as the laser power increases, the structures associated with $\Delta m_F = 1$ become less pronounced in the individual component signals and the difference signal. The signals do not show any visible dependence on the the precise hyperfine transition that is excited from a single ground-state hyperfine level. If the Zeeman splittings of an unknown atom or molecule are of interest, then the measurements of the circularity degree will clearly show whether the splitting is linear or nonlinear because the circularity degree is nonzero only when the magnetic splitting of Zeeman sublevels is nonlinear, and peaks in this signal will correspond to the crossings of magnetic sublevels. The level crossings are determined by the magnetic field value and two constants: magnetic moment and the hyperfine splitting constant. The analysis of level-crossing signals can help to determine these two constants for unknown atomic or molecular systems.

ACKNOWLEDGMENTS

We thank the Latvian State Research Programme (VPP) Project No. IMIS^2 and the NATO Science for Peace and Security Programme Project No. SfP983932 "Novel magnetic sensors and techniques for security applications" for financial support.

[1] M. Auzinsh, D. Budker, and S. Rochester, *Optically Polarized Atoms: Understanding Light-atom Interactions* (Oxford University Press, Oxford, 2010).

[2] D. Budker, W. Gawlik, D. F. Kimball, S. M. Rochester, V. V. Yashchuk, and A. Weis, Resonant nonlinear magneto-optical effects in atoms, Rev. Mod. Phys. **74**, 1153 (2002).

[3] Stephen E. Harris, Electromagnetically induced transparency, Phys. Today **50**(7), 36 (1997).

[4] D. F. Phillips, A. Fleischhauer, A. Mair, R. L. Walsworth, and M. D. Lukin, Storage of light in atomic vapor, Phys. Rev. Lett. **86**, 783 (2001).

[5] Chien Liu, Zachary Dutton, and Cyrus H. Behroozi, Observation of coherent optical information storage in an atomic medium using halted light pulses, Nature (London) **409**, 490 (2001).

[6] S. Knappe, P. D. D. Schwindt, V. Shah, L. Hollberg, J. Kitching, L. Liew, and J. Moreland, A chip-scale atomic clock based on ^{87}Rb with improved frequency stability, Opt. Express **13**, 1249 (2005).

[7] P. Yeh, Dispersive magnetooptic filters, Appl. Opt. **21**, 2069 (1982).

[8] Alessandro Cerè, Valentina Parigi, Marta Abad, Florian Wolfgramm, Ana Predojević, and Morgan W. Mitchell, Narrowband tunable filter based on velocity-selective optical pumping in an atomic vapor, Opt. Lett. **34**, 1012 (2009).

[9] L. Weller, K. S. Kleinbach, M. A. Zentile, S. Knappe, I. G. Hughes, and C. S. Adams, Optical isolator using an atomic vapor in the hyperfine paschen-back regime.Opt. Lett. **37**, 3405 (2012).

[10] Janis Alnis and Marcis Auzinsh, Angular-momentum spatial distribution symmetry breaking in Rb by an external magnetic field, Phys. Rev. A **63**, 023407 (2001).

[11] U. Fano, Precession equation of a spinning particle in nonuniform fields, Phys. Rev. **133**, B828 (1964).

[12] M. Lombardi, Note sur la possibilité d'orienter un atome par super-position de deux interactions séparément non orientantes en particulier par alignement électronique et relaxation anisotrope, C. R. Acad. Sci. Paris Ser. B **265**, 191 (1967).

[13] V. N. Rebane, Depolarization of resonance fluorescence during anisotropic collisions, Opt. Spectrosc. (USSR) **24**, 163 (1968).

[14] T. Manabe, T. Yabuzaki, and T. Ogawa, Observation of collisional transfer from alignment to orientation of atoms excited by a single-mode laser, Phys. Rev. Lett. **46**, 637 (1981).

[15] M. Auzinsh and R. Ferber, *Optical Polarization of Molecules*, Cambridge Monographs on Atomic, Molecular and Chemical Physics (Cambridge University Press, Cambridge, 2005).

[16] M. Lombardi, Création d'orientation par combinaison de deux alignements alignement et orientation des niveaux excités d'une décharge haute fréquence, J. Phys. (France) **30**, 631 (1969).

[17] Jean-Claude Lehmann, Étude de l'influence de la structure hyperfine du niveau excité sur l'obtention d'une orientation nucléaire par pompage optique, J. Phys. (France) **25**, 809 (1964).

[18] W. E. Baylis, Optical-pumping effects in level-crossing measurements, Phys. Lett. A **26**, 414 (1968).

[19] J. C. Lehmann, Nuclear orientation of Cadmium^{111} by optical pumping with the resonance line $5^1S_0 - 5^1P_1$, Phys. Rev. **178**, 153 (1969).

[20] M. Krainska-Miszczak, Alignment and orientation by optical pumping with pi polarised light, J. Phys. B **12**, 555 (1979).

[21] H. Brändle, L. Grenacs, J. Lang, L. Ph. Roesch, V. L. Telegdi, P. Truttmann, A. Weiss, and A. Zehnder, Measurement of the correlation between alignment and electron momentum in $^{12}\mathrm{B} \rightarrow {}^{12}\mathrm{C}$(g.s.) decay by a novel technique: another search for second-class currents, Phys. Rev. Lett. **40**, 306 (1978).

[22] M. Auzinsh, A.V. Stolyarov, M. Tamanis, and R. Ferber, Magnetic field induced alignment–orientation conversion: nonlinear energy shift and predissociation in te2b1u state, J. Chem. Phys. **105**, 37 (1996).

[23] S. Stenholm, *Foundations of Laser Spectroscopy* (Dover, New York, 2005).

[24] M. Auzinsh, D. Budker, and S. M. Rochester, Light-induced polarization effects in atoms with partially resolved hyperfine structure and applications to absorption, fluorescence, and nonlinear magneto-optical rotation, Phys. Rev. A **80**, 053406 (2009).

[25] Kaspars Blushs and Marcis Auzinsh, Validity of rate equations for zeeman coherences for analysis of nonlinear interaction of atoms with broadband laser radiation, Phys. Rev. A **69**, 063806 (2004).

[26] M. L. Harris, C. S. Adams, S. L. Cornish, I. C. McLeod, E. Tarleton, and I. G. Hughes, Polarization spectroscopy in rubidium and cesium, Phys. Rev. A **73**, 062509 (2006).

[27] J.P. Barrat and C. Cohen-Tannoudji, Élargissement et déplacement des raies de résonance magnétique causés par une excitation optique, J. Phys. Radium **22**, 443 (1961).

[28] M. I. D'yakonov, Theory of resonance scattering of light by a gas in the presence of a magnetic field, Sov. Phys. JETP **20**, 1484 (1965).

[29] M. Auzinsh, R. Ferber, I. Fescenko, L. Kalvans, and M. Tamanis, Nonlinear magneto-optical resonances for systems with J100 observed in K_2 molecules, Phys. Rev. A **85**, 013421 (2012).

[30] M. Auzinsh, A. Berzins, R. Ferber, F. Gahbauer, U. Kalnins, L. Kalvans, R. Rundans, and D. Sarkisyan, Relaxation mechanisms affecting magneto-optical resonances in an extremely thin cell: experiment and theory for the cesium D_1 line, Phys. Rev. A **91**, 023410 (2015).

[31] M. Auzinsh, R. Ferber, F. Gahbauer, A. Jarmola, and L. Kalvans, Nonlinear magneto-optical resonances at D_1 excitation of ^{85}Rb and ^{87}Rb for partially resolved hyperfine F levels, Phys. Rev. A **79**, 053404 (2009).